molecular pharmaceutics

Article

pubs.acs.org/molecularpharmaceutics

Forming of Demethoxycurcumin Nanocrystallite-Chitosan Nanocarrier for Controlled Low Dose Cellular Release for Inhibition of the Migration of Vascular Smooth Muscle Cells

Yen-Jen Wang,[†] Hui-Yi Lin,[‡] Chieh-Hsi Wu,[‡] and Dean-Mo Liu*[,†]

[†]Nano-Bioengineering Laboratory, Department of Materials Science and Engineering, National Chiao Tung University, Hsinchu 300, Taiwan

[‡]Department of Pharmacology, China Medical University, Taichung 404, Taiwan

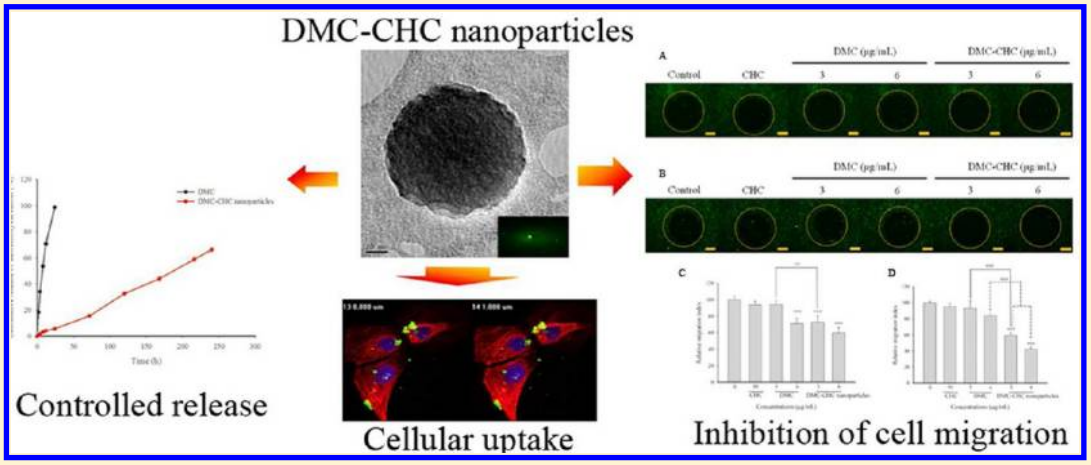

ABSTRACT: We report an efficient therapeutic approach to inhibit the migration and growth of vascular smooth muscle cells (VSMCs) via a low-dose sustained elution of a water-insoluble drug, demethoxycurcumin (DMC), through a self-assembled amphiphilic carbomethyl-hexanol chitosan (CHC) nanomatrix. Manipulating the cellular internalization and controlled cytotoxic effect of DMC-CHC nanoparticles over the VSMCs was elucidated. The DMC-CHC nanoparticles, which were systematically characterized in terms of structural morphology, surface potential, encapsulation efficiency, and DMC nanocrystallite distribution, exhibited rapid cellular uptake efficiency and considerably improved cytotoxic potency by 2.8 times compared to the free DMC. Under a cytotoxic evaluation, an improved antiproliferative effect and effective inhibition of VSMC migration as a result of highly efficient intracellular delivery of the encapsulated DMC in comparison to free DMC was achieved, which also was confirmed with a subsequent protein analysis. Cellular drug release and distribution of DMC after internalization into VSMCs was experimentally determined. This work may open a potential intracellular medicinal strategy with improved biological and therapeutic efficacy using the DMC-CHC nanoparticles illustrated in this work.

KEYWORDS: *amphiphilic chitosan, demethoxycurcumin, cellular drug release, vascular smooth muscle cell, cellular migration*

INTRODUCTION

Vascular smooth muscle cell (VSMC) migration is a process that occurs in the development of several vascular pathologies, including intimal hyperplasia and atherogenesis.[1] Artery wall remodeling, a major feature of diseases such as hypertension, restenosis, atherosclerosis, and aneurysm, involves changes in the tunica media mass that reduce or increase the vessel lumen.[2] Arterial injury causes VSMCs to transform from a contractile to synthetic state, migrate to the intima, proliferate, and produce extracellular matrix proteins, narrowing the artery lumen.[3]

Among those physiological disorders, the exaggerated proliferation and migration of the VSMCs have been considered playing a major role in the advanced development of damaged lesions, such as the most prominent examples of blood vessel narrowing or restenosis in the field of cardiovascular disorders.[4] In this prominent case, with increasing attention paid to the inflammatory process in injured arterial wall over the recent decade, it has been well recognized that a great extent of migration and exaggerated proliferation of VSMCs in the lumen predominates the narrowing of the injured artery.[5] Therefore, inhibition of VSMC proliferation and migration has becoming a crucial concern in medical and pharmaceutical communities over the years. Earlier studies have shown that pretreatment with

Received: March 19, 2012
Revised: June 13, 2012
Accepted: June 26, 2012
Published: July 13, 2012

antioxidants can significantly reduce balloon injury-induced neointima formation.[6,7] Until now, a number of therapeutic antiproliferative, antioxidant, and anti-inflammatory drugs have been reported to exert inhibitory efficacy toward the VSMCs,[8−10] although an optimal dosing has barely been quantitatively determined both *in vitro* and *in vivo*, especially under a sustained elution manner. One major hurdle is the poor bioavailability of those selected drugs as a result of poor physiological solubility, which has been addressed to considerably attenuate therapeutic efficacy of drugs. Therefore, a precise and optimal dosing of the drugs with suitable elution profile to modulate the inhibition of the VSMC migration and proliferation with greater efficacy remained a challenging task to be well manipulated.

Among those therapeutic substances, natural curcumin has been used for inhibiting VSMC migration and is virtually a mixture of three bis-*a*,*b*-unsaturated-*c*-diketone hydrophobic curcuminoids, included curcumin, demethoxycurcumin, and bisdemethoxycurcumin in a ratio of 77:17:3.[11−13] Curcuminoids are recognized for their broad spectrum of biological activities and safety in foods or pharmaceuticals.[14] As one of the most crucial features of curcuminoids is their strong antioxidative property, a study reported the strong antioxidant activity of demethoxycurcumin to be as efficient as the well-known strong antioxidant curcumin.[15] Previous reports suggested that curcuminoids are effective antiproliferative, antimigratory, antioxidant, and anti-inflammatory agents; however, poor bioavailability has hampered the desired therapeutic use of curcuminoids in a number of clinical trials.[16−18]

Among the derivatives of the curcuminoids, there have been no reports on investigating demethoxycurcumin as an antirestenotic agent *in vitro*. Being highly hydrophobic in nature, demethoxycurcumin is insoluble in water but soluble in solvents including ethanol, dimethyl sulfoxide, and acetone.[18] To increase its solubility and bioavailability, attempts have been made through encapsulation in liposomes and polymeric-based and lipid-based nanoparticles.[19−21] Among those colloidal drug carriers, biodegradable polymers have received greater attention recently for local release of drug toward the arterial wall.[22,23]

In this work, attempts to inhibit the migration and proliferation of smooth muscle cells, using VSMCs as model cell line, through the controlled release of demethoxycurcumin (DMC) were designed. To properly modulate the DMC elution, a highly biocompatible amphiphilic chitosan, which was previously developed in this lab, was employed as a drug carrier.[24] The amphiphilic chitosan is virtually a modified version of natural chitosan through carboxylmethylation (to replace 48% hydroxyl groups) and hexanoyl replacement (for 50% amine groups) along the backbone of pristine chitosan to form the modified chitosan (termed as CHC). Such a dual-ligand modification rendered the resulting modified chitosan to be highly dissoluble in aqueous solution of neutral pH and biocompatible, and it is capable of self-assembling to form well-defined nanocapsules in a number of water−solvent mixtures.[25] By taking the advantage of the CHC, here we focus more, as one of the main objectives of this communication, on the cellular behavior of the VSMCs in response to the compatible nature of the DMC-CHC nanoparticles and its corresponding biological activity in terms of the inhibition effect.

MATERIALS AND METHODS

3-(4,5-Dimethylthiazol-2-yl)-2,5-diphenyltetrazolium bromide (MTT), 4′,6-diamidino-2-phenylindole (DAPI), 2-propanol, rhodamine-phalloidin, sodium hydroxide, chloroacetic acid, fluorescein isothiocyanate (FITC), and phosphate buffered saline (PBS) were purchased from Sigma. Demethoxycurcumin was a courteous gift from China Medical University (Taiwan). The antibody against MAPK/extracellular signal-regulated kinase (ERK) 1/2, MMP-2, MMP-9, and phosphorylated proteins were purchased from Cell Signaling Technology (Beverly, MA). Anti-ERK1/2, antifocal adhesion kinase (FAK), antiphosphorylated focal adhesion kinase (p-FAK), and horseradish peroxidase-conjugated goat anti-mouse IgG antibody were purchased from Santa Cruz Biotechnology Co. (Santa Cruz, CA). All other chemical reagents in the study were analytical grade and used as received without further purification.

Preparation and Characterization of DMC-CHC Nanoparticles. The carboxymethyl-hexanoyl modified polymeric chitosan (termed as CHC) was purchased from Advanced Delivery Technologies. Inc. (Taiwan) and used without further purification. The CHC has been known to exhibit self-assembly behavior while dissolving in aqueous solution with physiological pH.[24] Demethoxycurcumin (DMC) and CHC were completely solubilized in methanol/ddH_2O (1:4 v/v), the methanol was removed under reduced pressure using a rotary vacuum evaporator at room temperature, and the resulting solution was then centrifuged at 10000*g* for 30 min to remove free DMC. The supernatant was filtered with a 0.8 μm syringe filter and lyophilized to give a yellow powder.

The morphological structure of the DMC-CHC nanoparticles was examined using transmission electron microscopy (TEM) (JEOL 2100, Japan). The TEM samples were prepared right after the DMC-CHC nanoparticles were synthesized, and each sample (1 mg/mL) was placed on a 300-mesh copper grid coated with carbon. After the sample was dried, negative staining was performed using a droplet of 2 wt % uranyl acetate, 30 min. The zeta potential and size of the nanoparticles (1 mg/mL in PBS) were determined by laser Doppler anemometry (Beckman Coulter, Inc., USA). All analyses were performed on samples appropriately diluted with PBS buffer in order to maintain a constant ionic strength.

Determination of Loading Efficiency. The loading efficiency of DMC in the DMC-CHC nanoparticles was measured by high-performance liquid chromatography (HPLC). Lyophilized DMC-CHC nanoparticles (1 mg) were dissolved in 1 mL amounts of methanol to obtain a clear solution. Then, drug concentration was quantified by HPLC, based on a standard concentration curve of free DMC in methanol. Isocratic reversed-phase HPLC was performed using a 1200 series HPLC system (Agilent Technologies, Wilmington, DE) with a C18 column (Zorbax eclipse, 5 μm, 4.6 × 150 mm). The mobile phase consisted of 50:50 (v/v) acetonitrile/0.3% formic acid (pH 3.0) and was delivered at a flow rate of 1.0 mL/min. Eluted compounds were detected at 425 nm using a Spectra100 UV−vis detector. The drug-loading efficiency (DLE, %) was calculated with the following equation.

$$\text{DLE}\,(\%) = [(\text{amount of DMC in nanoparticles}) / (\text{amount of DMC used for nanoparticle preparation})] \times 100 \quad (1)$$

dx.doi.org/10.1021/mp300150q | *Mol. Pharmaceutics* 2012, 9, 2268−2279

***In Vitro* Release Study.** A predetermined amount of lyophilized DMC-CHC nanoparticles (50 mg) was dispersed in 9 mL of PBS, pH 7.4, and the solution was divided into 30 eppendorf tubes (300 μL each). The tubes were gently shaken at 37 °C in an orbital shaker incubator at 100 rpm. Free DMC is completely insoluble in water; therefore, at predetermined time intervals, the solution was centrifuged at 5000 rpm for 30 min to separate the released DMC from the loaded DMC-CHC nanoparticles. The released DMC was redissolved in 300 μL of methanol, and 20 μL of this solution was injected in the HPLC to determine the amount of DMC released with respect to different time intervals. In the control, 1 mL of diluted solution of free DMC (containing 5% ethanol) with an equivalent amount of drug to DMC-CHC nanoparticles was evaluated by the dialysis method. A dialysis membrane tube (SnakeSkin, USA) filled with 1 mL of diluted free DMC solutions was immersed in 10 mL of PBS of pH = 7.4. The released DMC outside of the dialysis membrane tube was sampled at defined time period and assayed by HPLC. The percentage of DMC released at different time intervals was determined from the following equation.

$$\begin{aligned}&\text{released DMC (\%)}\\&= [(\text{released DMC from DMC} - \text{CHC nanoparticles})\\&\quad /(\text{total amount of DMC in DMC}\\&\quad - \text{CHC nanoparticles})] \times 100 \qquad (2)\end{aligned}$$

Cytotoxicity Assay. A10 vascular smooth muscle cells (VSMCs) from Food Industry Research and Development Institute (Hsinchu, Taiwan) were cultured in DMEM supplemented with 10% fetal bovine serum and 1% antibiotic antimycotic solution (Gibco, USA) in a humidified atmosphere containing 5% CO_2 in air at 37 °C.

The investigation of cell viability is a common method to evaluate the biocompatibility of biomaterials. The cytotoxicity of drug-free nanoparticles, free DMC, and DMC-CHC nanoparticles was evaluated using VSMCs by MTT colorimetric procedure. VSMCs were plated at 2×10^4 cells per well in a 24-well culture plate (Corning, USA) for 24 h to attach, followed by replacement of the sample solutions and incubation for a predetermined time. At a predetermined time, the medium containing samples was aspirated and the wells were washed twice using PBS solution. Then, MTT solution (0.5 mg/mL) was added and incubated for 4 h. The purple formazan was solubilized with isopropanol and measured in a microplate reader (TECAN Sunrise, Switzerland) at 595 nm.

Migration Assay. Evaluation of VSMC migration was performed as described[26] and with Oris cell migration assembly kit-flex (Platypus Technologies, Madison, WI) according to the manufacturer's instructions. In brief, Oris cell seeding stoppers were inserted into 96-well plates to prevent attachment of the cells in the center of the well (2 mm diameter). Then, when cells were confluent, the stoppers were removed and cells were treated with samples for 24 h. At the end point, cells were stained with 4 μg/mL Calcein AM for 30 min at 37 °C. Migration was evaluated by counting the number of cells in the denuded zone. Photographs were taken under phase contrast light microscopy (Nikon).

Fluorescence Confocal Microscopy. VSMCs were cultured on coverslips and incubated with or without FITC-DMC-CHC nanoparticles at a concentration of 5 μg/mL for predetermined time periods. After incubation, VSMCs were fixed with 3.7% formaldehyde and permeabilized with 0.1% Triton X-100. Cells were subsequently washed twice with PBS and incubated at room temperature with rhodamine-phalloidin overnight. After washing with PBS, cells were stained with DAPI for 1 h. Finally, coverslips were then mounted on glass slides by mounting solution (Dako) and observed by fluorescence confocal microscopy with Nikon C1 plus confocal system.

Cellular Uptake. A flow cytometer was employed to determine the internalization of FITC-CHC nanoparticles and FITC-DMC-CHC nanoparticles with the VSMCs; exponential growth of VSMCs was carried out. VSMCs were plated at 5×10^5 cells in a 10 cm dish and allowed to attach for 24 h. The culture medium was discarded, and the cells were washed with PBS. To examine the effect of incubating time, the cells were incubated with FITC-CHC nanoparticles and FITC-DMC-CHC nanoparticles for predetermined time periods at 37 °C, in order to determine the time-dependent cellular uptake of the nanoparticles. The amounts of FITC-DMC-CHC nanoparticles were equal in dose to the FITC-CHC nanoparticles. After the cellular uptake treatment, VSMCs were washed twice with PBS and then harvested by trypsinization. Then, VSMCs were centrifuged, collected, and dehydrated with 70% ethanol overnight at −20 °C (for fixed cells), followed by resuspending with PBS. To avoid cell aggregation, the cell solutions were filtered through a nylon membrane (BD Biosciences, USA). A minimum of ten thousand dead cells were analyzed. The cellular uptake of nanoparticles was determined by BD FACSCalibur flow cytometry, and the fluorescence intensity was quantified by CellQuest software CellQuest Pro software (BD Biosciences, USA).

Intracellular Localization of the DMC-CHC Nanoparticles. Assessment of colocalization of DMC-CHC nanoparticles in VSMCs was carried out by culturing the cells on glass coverslips for 24 h and then treatment with 5 μg/mL FITC-DMC-CHC nanoparticles for 4 h. Afterward, they were washed in ice-cold PBS and fixed for 15 min with 3.7% formaldehyde, and permeabilization was performed with 0.1% Triton X-100. To label late endosome or lysosome of cells using LysoTracker Red Lysosomal Probe (Lonza, USA), VSMCs were incubated with probe containing medium (50 nM) for 30 min at 37 °C. The cells were rapidly washed with ice-cold PBS and then fixed and mounted. Samples were then examined on a fluorescence microscope.

Intracellular Drug Distribution. To explore *in vitro* drug quantification/distribution of DMC-CHC nanoparticles after their internalization within the VSMCs, the cells were seeded on 24-well culture plates with a seeding density of 50,000 cells/well. After reaching confluence, wells were carefully washed with PBS buffer. Then the DMC-CHC nanoparticles at a concentration of 2 μg/mL were added along with the media in triplicate to the wells, incubated for different time intervals of 1, 2, 4, 12, and 24 h, respectively, and processed for quantification of DMC by HPLC at 425 nm. Sample preparation for intracellular drug distribution involves pelletization of DMC-CHC nanoparticles with cells at 12,000 rpm for 5 min, drying, and lysis of the pellet in methanol followed by probe sonication at higher amplitude for 5 min so that DMC can be extracted into the methanol fraction. The lysate was centrifuged at 10,000 rpm for 5 min, and HPLC was used to determine the amount of DMC released cellularly with respect to different time intervals.

Table 1. Characterizations of DMC-CHC Nanoparticles[a]

sample	initial amt of demethoxycurcumin (mg/mL)	loading efficiency (%)	zeta potential (mV)	size (nm)
DMC(0.05)-CHC	0.05	77.8 ± 0.8	−17.3 ± 2.0	93.2 ± 2.3
DMC(0.1)-CHC	0.1	74.3 ± 0.3	−13.5 ± 1.6	107.4 ± 6.8
DMC(0.2)-CHC	0.2	52.4 ± 1.9	−14.5 ± 4.0	175.4 ± 7.4

[a]Values are expressed as mean ± SD (n = 3).

Western Blotting Analysis. VSMCs cultured in six-well plates were incubated with DMC-CHC nanoparticles (containing DMC 1, 3, and 6 μg/mL) in DMEM containing 15% FBS for 24 h. Then, equal protein contents of total cell lysate from control and DMC-CHC nanoparticle-treated sample were resolved by denaturing sodium dodecyl sulfate−polyacrylamide gel electrophoresis (SDS−PAGE) using standard methods and then were transferred onto polyvinylidene fluoride membranes (Millipore, Bedford, MA, USA) by electroblotting. Nonspecific binding of the membranes was blocked with phosphate-buffered saline (PBS) containing 5% (w/v) nonfat dry milk and TBS-T buffer (Tris-Buffer Saline with 0.1% (v/v) Tween 20) for more than 1 h. Membranes were washed with TBS-T buffer three times each for 10 min and then probed with the primary antibodies overnight at 4 °C. After washing the membrane three times for 10 min in TBS-T buffer, the membranes were then incubated with horseradish peroxidase-conjugated secondary antibody for 1 h at 37 °C. The membranes were washed three times, and the immunoreactive proteins were detected by enhanced chemiluminescence (ECL) using hyperfilm and ECL reagent (Amersham International PLC, Buckinghamshire, U.K.).The results were quantified using Kodak Molecular Imaging (MI) software and expressed as relative intensity compared with control.

Statistics Analysis. The data was compared between groups of inhibitory of migration, cytotoxicity assay, and Western blotting analysis using one-way analysis of variance. All other data were normally distributed, and therefore Student's t-test was used. A value of $p < 0.05$ was considered statistically significant.

RESULTS

Characterization of the DMC-CHC Nanoparticles. Table 1 gives a number of physical parameters for the DMC-CHC nanoparticles prepared in this work. The resulting DMC-CHC nanoparticles exhibited a negative zeta potential, which appeared to be relatively constant at about −15 mV, irrespective with the drug loads, indicating the DMC, dissolved in the methanol/ddH_2O (1:4 v/v) phase, exerted no additional charge effect to the CHC nanomatrix upon self-assembly. The loading efficiency of DMC-CHC nanoparticles was determined by varying loading amounts of DMC while the CHC was kept constant. Drug loading characteristics of the nanoparticles are summarized in Table 1. The drug loading efficiency was determined ranging from 77.8% ± 0.8% to 52.4% ± 1.9% depending upon the starting DMC concentration from 0.05 mg/mL to 0.2 mg/mL, respectively. This suggests that DMC molecules are entrapped into the hydrophobic regions of the CHC upon self-assembly and the entrapped DMC molecules caused an increase, by a factor of 1.88, in the size of the CHC nanomatrix, from 93.2 to 175.4 nm, with initial DMC concentration increased by a factor of 4, from 0.05 mg/mL to 0.2 mg/mL, respectively. Although the drug load efficiency is likely to reduce, the drug payload showed a 3-fold increase from 0.039 mg/mL to 0.105 mg/mL, with increasing drug concentration, from 0.05 mg/mL to 0.2 mg/mL, respectively. Such an increase of drug payload is pharmaceutically and medically beneficial over practical applications.

The chemical structures of DMC and CHC are given in Figure 1. Following TEM examination, Figure 1 shows a spherical morphology of the resulting DMC-CHC nanoparticle, having a size of about 150 nm. A closer examination of the nanoparticle revealed numerous white spots, having a size of 2−3 nm, interdistributed with dark regions throughout the nanoparticles. Electron diffraction pattern on those white spots, inset in Figure 1, indicates a slight crystalline character, which is believed to be DMC crystallites. This finding suggested the DMC molecules being crystallized and distributed randomly throughout the molecular framework of the CHC nanomatrix.

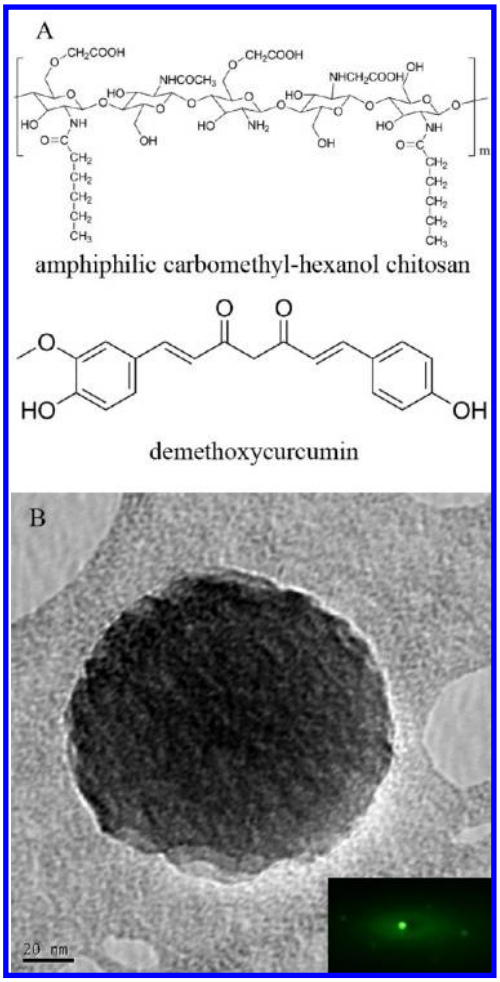

Figure 1. (A) Structural formulas of the amphiphilic carbomethyl-hexanol chitosan and demethoxycurcumin. (B) TEM images and corresponding electron diffraction pattern (inset) of DMC-CHC nanoparticles (scale bar: 20 nm).

dx.doi.org/10.1021/mp300150q | Mol. Pharmaceutics 2012, 9, 2268−2279

***In Vitro* Release.** A release experiment of DMC-CHC nanoparticles with an equivalent amount of drug to that control experiment (free DMC), carried out under the same conditions at 37 °C, indicated that the dialysis membrane played a negligible role in the release of DMC. But the dialysis technique is a cumbersome setup procedure for dialysis bags and membrane at one end of a tube.[27] *In vitro* release from DMC-CHC nanoparticles can be directly assessed through materials and methods. This technique provides a direct and reasonably accurate assessment of *in vitro* release. *In vitro* release profiles of free DMC and DMC-CHC nanoparticles were investigated in PBS at 37 °C as shown in Figure 2 where

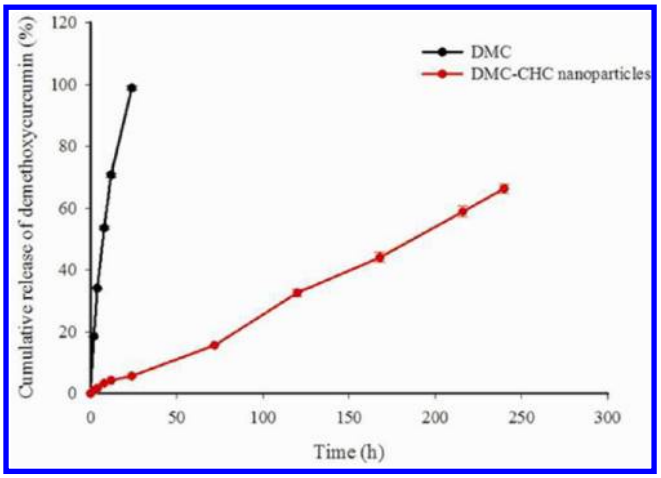

Figure 2. *In vitro* demethoxycurcumin release profiles from DMC-CHC nanoparticles (red line), in comparison with free demethoxycurcumin (black line) in PBS (pH 7.4, 37 °C). The release profiles of DMC-CHC nanoparticles were measured by absorption at 425 nm with HPLC. Each data point is represented as mean ± SD (n = 3). Error bars represent standard deviation.

free DMC was completely eluted in 24 h, while a sustained, slow profile for a time period of 10 days (corresponding to an accumulative amount of about 65%) was determined for the DMC-CHC nanoparticles. This observation confirmed that the CHC nanoparticles should act as an effective physical barrier against the free diffusion of entrapped DMC. More, as aforementioned, the DMC exists in a form of nanocrystallite (Figure 1), and a slow dissolution rate of the DMC nanocrystallite may also contribute to the observed sustained release profile.

***In Vitro* Cytotoxicity.** The cytotoxicity of the free DMC and DMC-CHC nanoparticles toward VSMCs was evaluated by the MTT assay. The CHC nanomatrix (in a concentration range of 5−50 μg/mL) were incubated as a control with VSMCs for 24 h, 48 h, and 72 h. Cell viability remained above 94%, indicating that the CHC nanomatrix was relatively biocompatible with VSMCs (Figure 3A) and can be a selective candidate for drug delivery applications. Cytotoxicity of free DMC and DMC-CHC nanoparticles of various concentrations with respect to VSMCs is given in Figure 3B. VSMCs were incubated with the DMC-CHC nanoparticles at an equivalent dose as the free DMC. Free DMC significantly decreased the viability of VSMCs in a dose-dependent manner while the DMC-CHC nanoparticles also inhibited the growth of VSMCs at a predicted concentration. Based on the dose-dependent controlled cytotoxic profiles, the inhibition concentration IC_{50} was calculated for the free DMC and the DMC-CHC

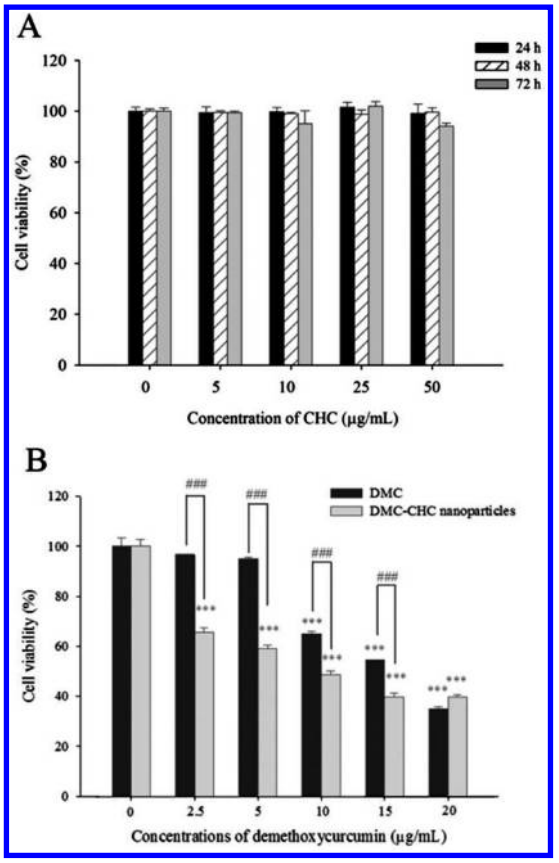

Figure 3. (A) *In vitro* cytotoxicity toward VSMCs of CHC for 24 h, 48 h, and 72 h and (B) DMC and DMC-CHC nanoparticles in 24 h incubation was evaluated by MTT assay. Each data point is represented as mean ± SD (n = 3). Error bars represent standard deviation. *** $p < 0.001$ compared to control (0 μg/mL).

nanoparticles, giving a value of 16.2 and 6.1 μg/mL respectively, indicating an improved potency by nearly 2.8 times for the encapsulated DMC. In the literature, curcumin has revealed its great potency in anti-restenosis therapeutics;[12] from our current study, the DMC has not only demonstrated a strong IC_{50} to VSMCs but also improved significantly in its cytotoxicity after being encapsulated into the CHC nanomatrix. This improvement not only is believed a result of rapid cellular internalization but also revealed a considerably improved potency while the DMC is directly released into the cell.

Migration Assay. As of prime consideration of this work, the DMC was designed to inhibit the growth, proliferation, and especially the migration of VSMCs via a sustained release approach, since it has been well recognized that exaggerated migration of the VSMC of the blood vessel takes major responsibility for neointima hyperplasia development along the damage lesions. Migration was evaluated by quantitating the number of cells that were able to migrate into a central denuded zone using the Oris Cell Migration assay kit (Platypus Technology, Madison, WI). As shown in a representative experimental outcome in Figure 4A, by treating with free DMC and DMC-CHC nanoparticles (with a high dose [6 μg/mL] and low dose [3 μg/mL] of DMC, a level equal to and lower than the IC_{50} dose) for 24 h, the migration of VSMCs was significantly retarded as shown by the delayed wound closure. Analysis was performed by cell number in the denuded zone. Figure 4C indicates that the DMC-CHC nanoparticles illustrated a greater inhibitory effect on cell mobility (60%,

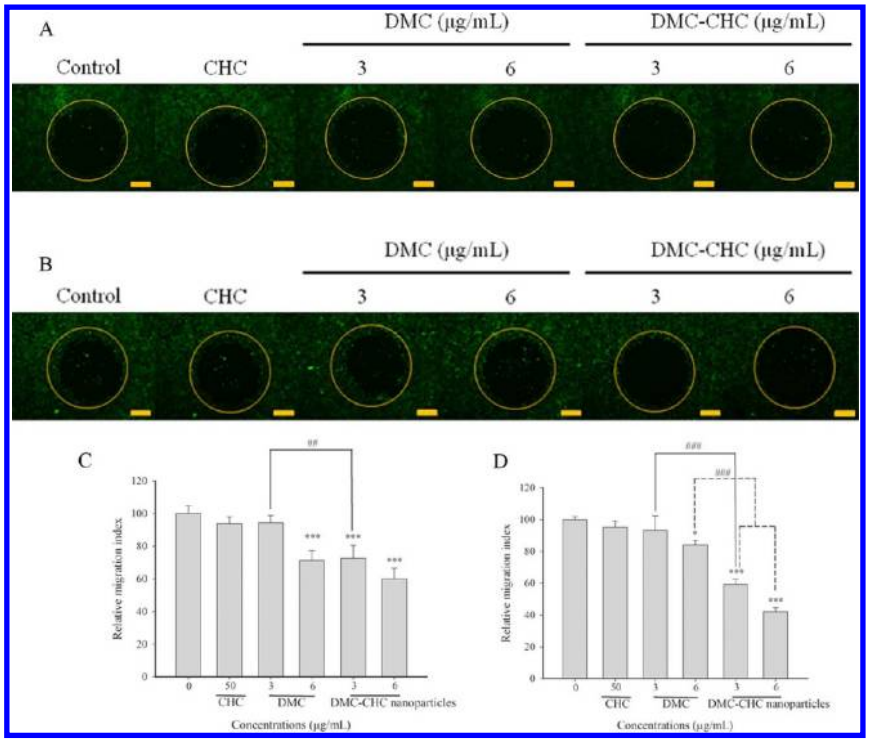

Figure 4. Inhibitory effects of DMC and DMC-CHC nanoparticles on cell migration of VSMCs. (A) Cell migration was examined at 0 and 24 h after treatment by the Oris Cell Migration Assay. (B) Cell migration was examined at 0 and 48 h after treatment by the Oris Cell Migration Assay. (C, D) Quantitative assessment of the percent of closure according to the mean number cells in the denuded zone at 24 and 48 h. * $p < 0.05$ and *** $p < 0.001$ compared to control (0 μg/mL); ## $p < 0.01$ and ### $p < 0.001$ compared to nanoparticles. Each data point is represented as mean ± SD ($n = 3$). Error bars represent standard deviation (scale bar: 500 μm).

72%) after 24 h incubation than free DMC (71%, 94%) at high dose and low dose, respectively (## $p < 0.01$ low concentration compared; *** $p < 0.001$ compared to control). After 48 h incubation, the results showed that the DMC-CHC nanoparticles at low-dose formulation had better inhibitory effect on VSMC migration than free DMC at high-dose formulation (Figure 4B). Figure 4D indicates that the DMC-CHC nanoparticles illustrated a greater inhibitory effect on cell mobility (42%, 59%) after 48 h incubation than free DMC (83%, 93%) at high-dose and low-dose formulation, respectively (* $p < 0.05$ and *** $p < 0.001$ compared to control; ### $p < 0.001$ compared to nanoparticles). However, CHC itself exerted a negligible effect on the migration of VSMCs compared to the control group.

Fluorescence Confocal Microscopy. Through FITC labeling, endocytosis of the DMC-CHC nanoparticles entrapped into VSMCs was further monitored by confocal microscopy to characterize the intracellular dynamics. The fluorescence images are displayed in Figure 5A. The merged image was the overlapping image obtained by DAPI channel (blue, nuclei), rhodamine channel (red, F-actin), and FITC channel (green, nanoparticles). Green fluorescence spectrum was observed inside the VSMCs after 4 h incubation with an equivalent dose of the FITC-DMC-CHC nanoparticles (5 μg/mL). FITC-DMC-CHC nanoparticles were clearly observed inside the cells as green dots. This observation confirmed that the FITC-DMC-CHC nanoparticles were internalized by VSMCs within 2 h of incubation, appearing in a punctate pattern around the nuclei, indicating that the DMC-CHC nanoparticles were largely and efficiently taken by the cells, which also proved the intracellular DMC distribution depicted in Figure 5A. Furthermore, Z-series images revealed that the FITC-doped nanoparticles were mainly distributed within the cytoplasm (Figure 5B). The DMC-CHC nanoparticles exhibited an exceptionally effective inhibition of migration and excellent uptake efficiency to the VSMCs, making a greater potency for inhibiting the growth and migration of the VSMCs.

Cellular Uptake. To further quantify the cellular uptake of the nanoparticles in cells, the fluorescence intensity in the cells after incubation with the FITC-CHC and FITC-DMC-CHC nanoparticles was determined by flow cytometry. Upon treatment with 25 μg/mL FITC-CHC nanomatrix in VSMCs for 8 h, the green fluorescence intensity was elevated in a time-dependent manner (Figure 6A); similar behavior was displayed with the FITC-DMC-CHC nanoparticles (containing 5 μg/mL DMC) (Figure 6B). The proportional amount of the FITC-CHC nanomatrix taken by the cells (M1) was very much the same over time periods of 0.5 h, 1 h, 2 h, 4 h, and 8 h corresponding to 92.9%, 95.9%, 96.0%, 97.2%, and 98.4%, respectively. The VSMCs also internalized the FITC-DMC-CHC nanoparticles in an efficient way, showing the accumulated nanoparticles for 0.5 h, 1 h, 2 h, 4 h, and 8 h corresponding to 94.5%, 94.2%, 95.4%, 96.2%, and 98.2%, respectively (Figure 6C). Upon analyzing 10,000 events using the FITC-CHC nanomatrix, the fluorescence intensity displayed an equal value compared with FITC-DMC-CHC nanoparticles. The results proved a similar internalization of the FITC-CHC nanomatrix by VSMCs and that of FITC-DMC-CHC nanoparticles, as illustrated in Figure 6D.

Intracellular Localization of the DMC-CHC Nanoparticles. Generally, the cellular uptake of nanoparticles is completed by enclosing them into endosomes. The early endosomes mature into late endosomes or multivesicular bodies, and then to lysosomes, which accompanies a significant

dx.doi.org/10.1021/mp300150q | Mol. Pharmaceutics 2012, 9, 2268−2279

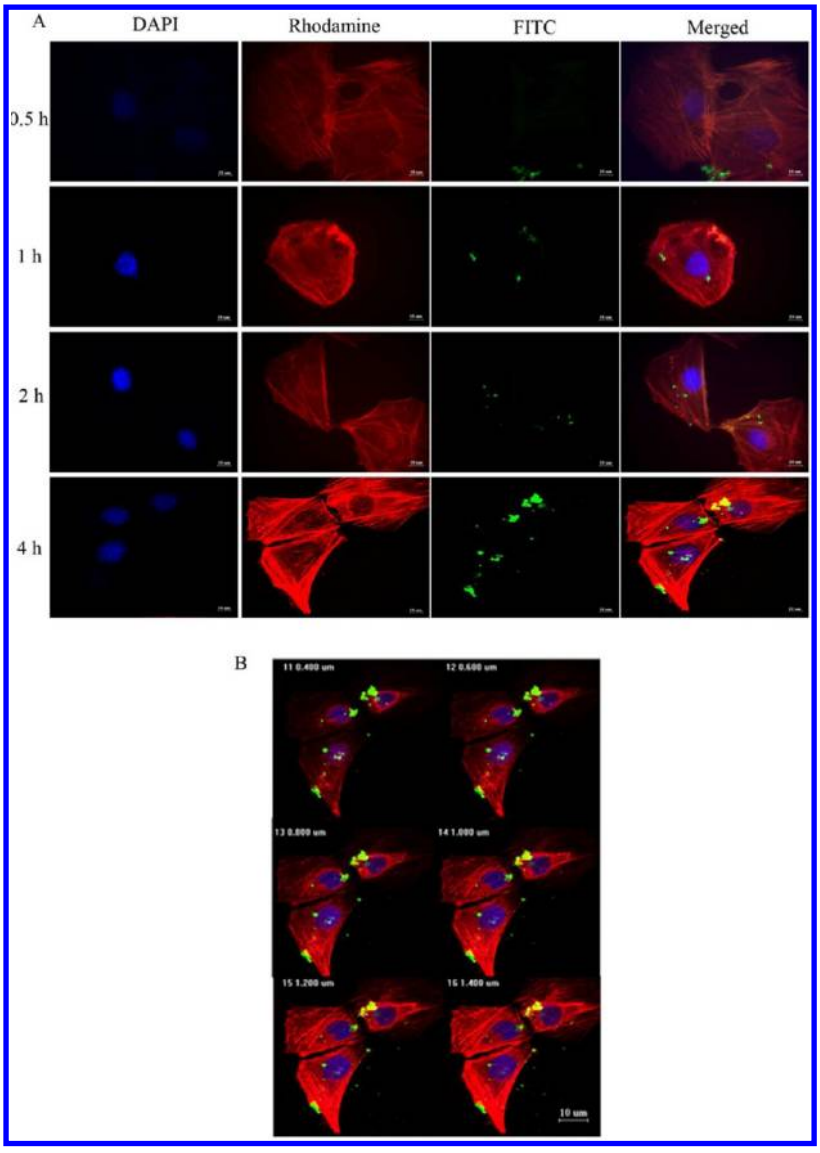

Figure 5. (A) Fluorescence images of VSMCs incubated with the DMC-CHC nanoparticles (5 μg/mL) for 0−4 h. The merged image was the overlapping image obtained by DAPI channel (blue, nuclei), rhodamine channel (red, F-actin), and FITC channel (green, nanoparticles). (B) Serial fluorescence Z-section images of VSMCs incubated with DMC-CHC nanoparticles (5 μg/mL, 4 h incubation). The images show that most nanoparticles are localized in the cytoplasm of VSMCs. Bar = 10 μm.

drop in pH.[28] Understanding the intracellular localization within the endolysosomal network and the fate of nanoparticles with respect to their uptake pattern is crucial in designing a new macromolecular carrier.[29] Unfortunately, elucidation of the exact intracellular trafficking pathway of nanoparticles is difficult due to the dynamics of maturation and traffic between endosomal and lysosomal compartments.[28] A high geometrical coincidence was observed between the lysotracker and the FITC-DMC-CHC nanoparticles (Figure 7A) under the confocal microscope, confirming the intracellular distribution to be primarily in the lysosomes. The position of nucleus in each cell was labeled with DAPI staining. Here, the colocalization of lysosome with FITC-DMC-CHC nanoparticles produced a yellow fluorescence in merged images. Upon its sustained release nature of the DMC-CHC nanoparticles, the elution of the DMC into the enzymatic environment of the lysosomes or directly into the cell cytoplasm should, indeed, exert an important impact on the pharmacological activity.

Intracellular Drug Distribution. Cellular DMC release was determined by treating the VSMCs with DMC-CHC nanoparticles (with DMC dose at 2 μg/mL, which was designed to exert less cytotoxicity toward the VSMCs according to Figure 3B) in methanol to lyse the cells so that the drug eluted within the cells can be quantified by HPLC. Figure 7B shows the drug release profile inside the cells, wherein DMC concentration is increased with incubation time, which also contributed as a result of cellular internalization of the nanoparticles.

MMP-2 and MMP-9 are known to be involved in the control of VSMC proliferation and migration into the intima.[30] Biological analysis, Figure 8, clearly reveals that the DMC-CHC nanoparticles could effectively downregulate p-FAK, p-ERK1/2, MMP-2, and MMP-9 expression in VSMCs. However, for CHC alone, no appreciable sign of the downregulating expression for these two proteins was detected (data not shown). Both the FAK and ERK1/2−MAPK were

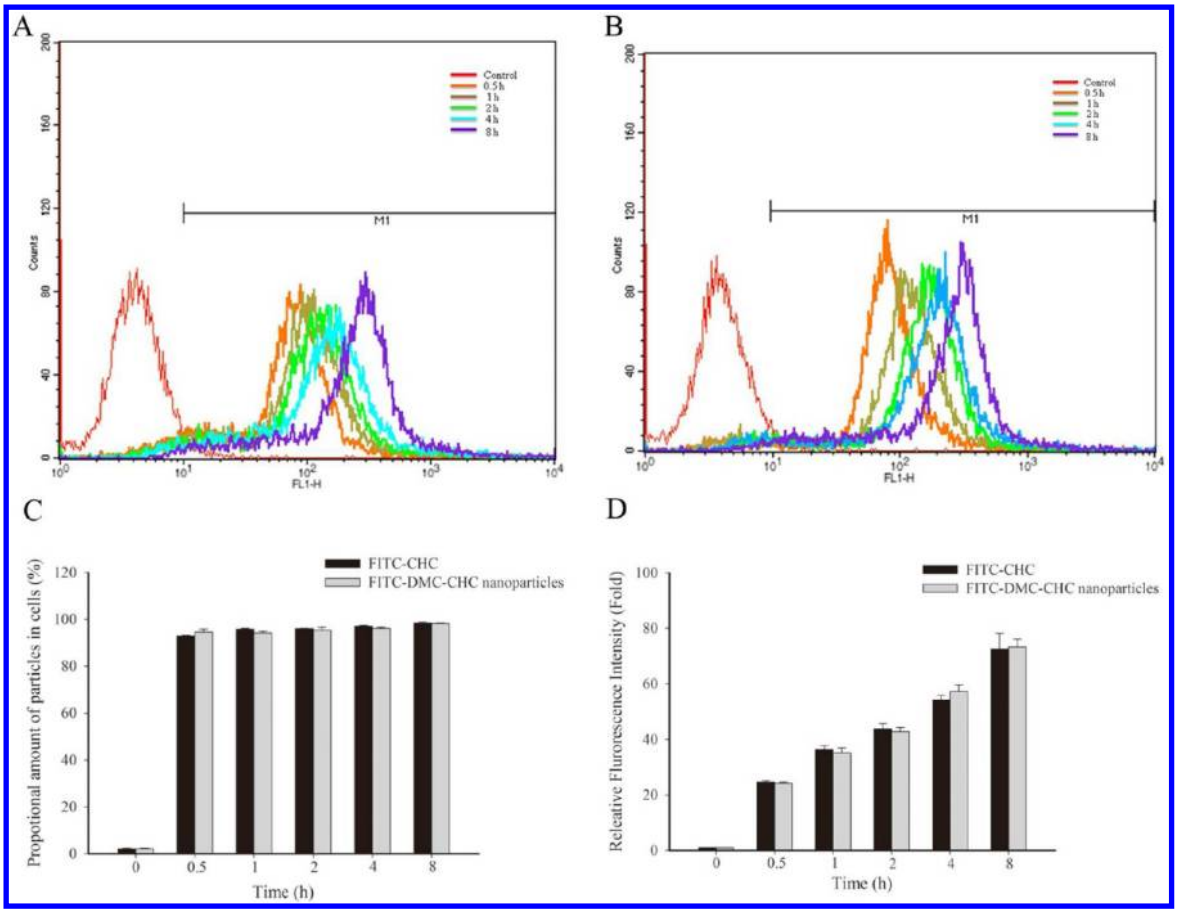

Figure 6. Cell uptake efficiency measured by flow cytometry analysis for (A) 25 μg/mL FITC-CHC and (B) 5 μg/mL FITC-DMC-CHC nanoparticles in VSMCs. VSMCs were treated with or without FITC-DMC-CHC nanoparticles for 0−8 h. At the end of treatment, the cells were trypsinized and then subjected to flow cytometer analysis. (C) Comparison of proportional amount of particles and (D) relative fluorescence intensity with FITC-CHC and FITC-DMC-CHC nanoparticles in VSMCs (M1). Analysis with flow cytometer by 10,000 cells was randomly selected for imaging analysis. Each data point is represented as mean ± SD (n = 3). Error bars represent standard deviation.

apparently not being affected by the presence of DMC-CHC nanoparticles.

DISCUSSION

Synthetic[31−33] and chemically modified natural[34−36] polymers have been actively exploited in drug delivery systems in order to address limitations of poor drug solubility, rapid *in vivo* clearance, insufficient target binding, and unwanted side effects.[37,38] However, the use of a polymer-based particle affords an additional and unique delivery opportunity where the particle acts as an intracellular depot, and delivers drug in a controllable manner around or within the cells. Following this study, it is clear that the amphiphilic derivatives of chitosan have been extensively studied in comparison with other polysaccharides.[39] This modified amphiphilic chitosan has demonstrated the ability to self-associate in contact with aqueous media to form polymeric nanoparticles and hydrogels.[40,41] Such structures can be used for the encapsulation and the release of active drugs.

The resulting DMC-CHC nanoparticles exhibited a negative zeta potential. The negative surface charge should be resulting from a deprotonation of the carboxyl groups ($-COO^-$), residing along the outer face of the nanoparticles, under physiological pH. Structural morphology of the DMC-CHC nanoparticles is illustrated in Figure 1A. The white spots were distributed randomly in the resulting nanoparticle. The SAED pattern suggested they were crystallites. Although it is hard to clearly define the crystalline structure of the white spots, it is presumed to be a distribution of the DMC molecule, having a molecular size close to 1 nm in length, associated with micropore evolution due to expulsion of aqueous phase surrounding the DMC after self-aggregation upon encapsulation. Nanocrystallite synthesis is a promising technology for poorly water-soluble drug delivery, which renders a much higher dissolution rate due to a larger specific surface area toward environmental medium. This has been demonstrated according to the Gibbs−Thomson equation,[42] contributing to faster dissolution *in vivo*.

Though apparently simple, the nanoprecipitation process is not yet clearly understood or well controlled. In this case, nanoprecipitation of the DMC inside the CHC matrix was achieved by mixing a solvent (methanol) and an antisolvent (water). As the solvent and antisolvent mixed, the DMC solution became supersaturated and started to precipitate out within the matrix. In classical nucleation theory, small but crystalline nuclei evolve first, and then further grow and agglomerate into final crystalline drug particles. Smaller DMC nanocrystallite (2−3 nm) precipitated in the CHC nanomatrix should be a result of spacious restriction of the surrounding CHC molecular network. For polymer matrix, three mechanisms included erosion, diffusion, and swelling by which the release of drug molecules can be controlled.[43] In Figure 2,

dx.doi.org/10.1021/mp300150q | *Mol. Pharmaceutics* 2012, 9, 2268−2279

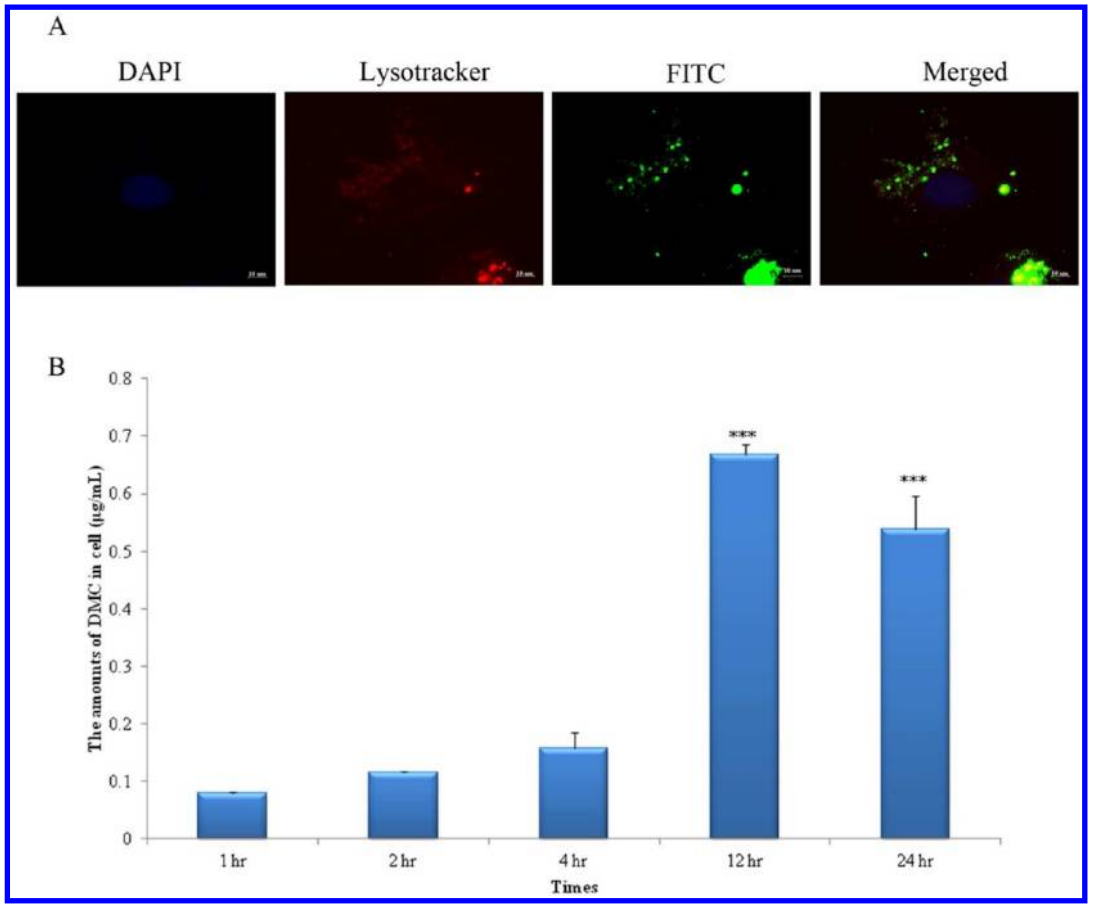

Figure 7. (A) Colocalization of green fluorescent FITC-DMC-CHC nanoparticles with late endosomes/lysosomes with LysoTracker Red and (B) cellular DMC release and distribution within the A10 VSMCs after internalization of the DMC-CHC nanoparticles at different time intervals. Each data point is represented as mean ± SD (n = 3, *** p < 0.001 compared to 1 h). Error bars represent standard deviation. Bar = 10 μm.

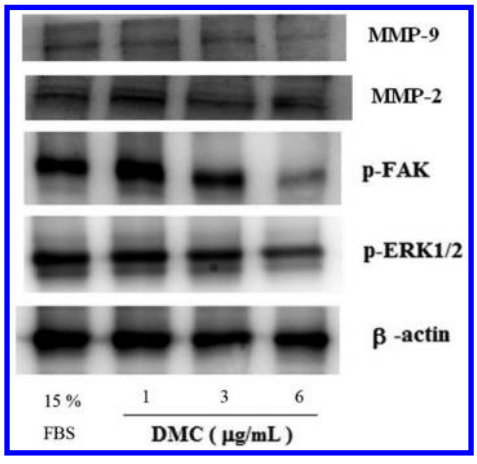

Figure 8. Concentration-dependent effects of DMC-CHC nanoparticles on the protein expression level of phosphorylated ERK1/2, phosphorylated AKT, MMP-2, and MMP-9. In the concentration-dependent assay, vascular smooth muscles were treated with 1, 3, and 6 μg/mL of DMC-CHC nanoparticles for 24 h. β-Actin was used as a loading control. The values indicate the density proportion of each protein compared with control.

DMC release is relatively fast for free DMC in a 24 h period compared to that of the DMC-CHC nanoparticles, wherein for the latter, from Figure 2, about 4.3% of the drug was released over 12 h of duration and reached about 6% at 24 h, followed by a much slower and almost constant release rate for the rest of the release time. The release profile appeared to follow a swelling-controlled mechanism, especially in the 12 h early phase release from the DMC-CHC nanoparticles. After the early phase release, the swelling of the nanoparticles may reach equilibrium, after which a linear diffusion-controlled mechanism followed. In comparison, early phase release demonstrated a higher release rate which is attributed to the DMC resided near the surface regions of the nanoparticles. Once being eluted to a certain extent, after a 12 h period, a sustained and linear release kinetic dominated as a result of slow diffusion, possibly associated with dissolution.

Inhibition of VSMC proliferation is an important strategy to prevent or halt the development of atherosclerosis. Curcumin, a nutrient supplement, has recently been demonstrated of such potential in literature.[44] The DMC-CHC nanoparticles demonstrated a much greater inhibition of VSMC proliferation than that of free DMC during a dose−response study, over a 24 h treatment (Figure 3b). Previous investigation reported that apoptosis was not observed in human umbilical vein endothelial cells (HUVEC) when DMC concentration was 15 μM (5.1 μg/mL).[45] These results demonstrated that DMC would inhibit the growth of VSMCs rather than endothelial cells at concentrations below 6 μg/mL (Figure 3b). This confirmed that DMC with optimal dose could inhibit the proliferation and migration of VSMCs into the arterial intima while exerting little or no adverse effect on the growth of vascular endothelial cells.

Taking the advantage of photochemical properties of DMC, the intracellular uptake of DMC-CHC nanoparticles compared

with free DMC was characterized using fluorescence confocal microscopy. Figure 5 indicates FITC-DMC-CHC nanoparticles being internalized efficiently by VSMCs. As a result, an increase in fluorescence intensity with time was observed for FITC-DMC-CHC nanoparticles within the VSMCs, indicating encapsulated DMC slowly released from the nanoparticles for a longer period of time. However, the DMC concentration for the cells treated with free DMC could hardly be determined by HPLC at any time intervals during the test. Associated with Figure 3b, we presumed that the free DMC may be prohibited or become much slower in being taken into the cells. However, after being encapsulated into the CHC nanomatrix, the resulting DMC-CHC nanoparticles bring a huge therapeutic benefit toward the targeted cells and an improved therapeutic efficacy can then be predicted for practical uses.

In order to investigate the antimetastatic effect in VSMCs, an inhibitory of migration assay was used. Speaking of restenosis, previous studies have also proved the significant role in VSMC migration, from the media into the intima, following arterial injury, and it has been widely accepted that blocking the migration of the VSMCs can reduce the neointimal lesion size.[46,47] To this point, cell migration is considered as an important key contributor to restenosis. The migration of VSMCs treated with CHC nanomatrix indicated that the CHC itself was nontoxic to inhibit the growth and migration of cells, while either free DMC or DMC-CHC nanoparticles alone were found to inhibit over a significant extent the migration of VSMCs over 24−48 h of treatment. The DMC-CHC nanoparticles exhibited the greatest inhibitory effect on cell mobility compared to free DMC at the same dose. One plausible explanation is due to rapid cellular internalization for the DMC-CHC nanoparticles rendering DMC released dominantly inside the cells that effectively deteriorated cell mobility, while the free DMC was exhausted rapidly after extensive exposure to the cells. The experimental observations indicated that the medical potential of the DMC-CHC nanoparticles prepared in this work can make them useful as candidates for sustained DMC delivery for a number of dose-dependent medications from anti-restenosis to anticancer therapy. A low-dose sustained release of the DMC from current design is more beneficial to treat uncontrollable growth and migration of VSMC-induced complications.

The size of the intracellular vesicles containing the endocytosed nanoparticles may give important information regarding the uptake mechanism.[48] Particle size and shape are two of the important factors for the cellular membrane surface to recognize and eventually internalize through the cellular pathways.[49] The CHC nanomatrix (∼150 nm in average) exhibited a size similar to DMC-CHC nanoparticles. Therefore, DMC-CHC nanoparticles could be efficiently internalized by VSMCs, still carrying a sufficient dose of DMC, released into cytosol, to effectively inhibit cell migration.

Internalization of nanoparticles occurs through various processes, such as macropinocytosis, clathrin-mediated endocytosis, and caveolae-mediated endocytosis. It is identifiable that these nanoparticles entered VSMCs by the pathways of clathrin-mediated endocytosis. Clathrin-mediated endocytosis (for nanoparticles in the size of ∼120 nm) is the most important mechanism occurring constitutively in all mammalian cells[50] and was recently found to be a dominantly internalizing mechanism for the CHC nanomatrix.[41] Reports showed that the clathrin-mediated endocytosis pathway is initiated by a specific ligand receptor interaction on the extracellular surface.[29] Upon entry, internalized nanoparticles were generally entrapped in the intracellular vesicles (i.e., endosomes), while some, through clathrin-mediated endocytosis, led to a complete degradation of macromolecular carriers at the later lysosomal stage.[29,51] Upon rapid internalization, the efficient endocytic mechanism permitted an efficient cellular release of DMC into the cells to effectively inhibit the migration and growth of the VSMCs.

In the literature, the results showed the protein signaling pathways (Erk1/2−MAPK and MMPs) are related to the inhibition of VSMC migration.[52] The production of MMP-9 and MMP-2 and smooth muscle cell migration should play key roles in the pathogenesis of neointima formation and atherosclerosis.[52] Although MMP-2 and MMP-9 have similar substrate specificities, the regulation of their expression is different. MMP-2 is constitutively expressed in several cell types, including VSMCs, and its expression is not induced by cytokines or growth factors.[52] In contrast, MMP-9 can be induced by TNF-α in VSMCs.[52] FAK protein has also been indicated to promote several cellular responses such as cell proliferation, adhesion and migration.[53] DMC-CHC nanoparticles significantly attenuated the levels of p-FAK proteins. In the present study, FAK protein was obviously decreased on cultured VSMCs, which could partially explain the cellular phenomenon of DMC-CHC nanoparticles on cell proliferation and migration of VSMCs. The ERK1/2−MAPK pathway generally participates in cell proliferation and survival signaling.[54] Our result showed that p-ERK1/2, p-FAK, MMP-2 and MMP-9 on cultured VSMCs can be markedly attenuated by DMC-CHC nanoparticles, Figure 8, which is in excellent agreement with the inhibition effect aforementioned.

■ CONCLUSION

A new pharmaceutical nanoformulation based on demethoxycurcumin (DMC)-loaded amphiphilic chitosan (termed CHC) nanomatrix was designed and characterized for investigation of cellular internalization and inhibitory effect on migration and growth of vascular smooth muscle cells. After encapsulation, DMC presented in a form of nanocrystallites distributed throughout the CHC nanomatrix, giving a size ∼150 nm in diameter. The resulting DMC-CHC nanoparticles were efficiently taken up by the VSMCs followed by a cellular sustained release inside the cells, with a maximal dose observed, 0.65 μg/mL, after 12 h of internalization. Compared with free DMC, the encapsulated DMC showed nearly 2.8 times higher potency and excellent inhibition effect on the migration and growth of the VSMCs via a low-dose elution profile. The cellular drug release profile proved the inhibition effect can be effectively triggered with relatively low DMC dose, compared to that of extracellular dose. This study may open a new therapeutic strategy using the highly cell-friendly CHC nanomatrix with low-DMC releasing doses to treat VSMC-induced complications.

■ AUTHOR INFORMATION

Corresponding Author

*National Chiao Tung University, Nano-Bioengineering Laboratory, Department of Materials Science and Engineering, 1001 Ta-Hseuh Road, Hsinchu 30049, Taiwan. Tel: +886-5712121 ext 55391. Fax: +886-3-5724727. E-mail: deanmo_liu@yahoo.ca.

Notes

The authors declare no competing financial interest.

■ ACKNOWLEDGMENTS

The project is supported by the National Chiao Tung University, Taiwan under Contract No. NSC 100-2622-M-009-002-CC3.

■ ABBREVIATIONS USED

VSMCs, vascular smooth muscle cells; DMC-CHC nanoparticles, demethoxycurcumin-loaded amphiphilic chitosan nanoparticles; CHC, amphiphilic carbomethyl-hexanol chitosan; HPLC, high-performance liquid chromatography; VSMCs, vascular smooth muscle cells; FITC, fluorescein isothiocyanate; FITC-CHC nanoparticles, FITC labeled CHC nanoparticles; MTT, 3-(4,5-dimethylthiazol-2-yl)-2,5-diphenyltetrazolium bromide; FITC-DMC-CHC nanoparticles, FITC labeled demethoxycurcumin-CHC nanoparticles

■ REFERENCES

(1) Willis, A. I.; Pierre-Paul, D.; Sumpio, B. E.; Gahtan, V. Vascular smooth muscle cell migration: current research and clinical implications. *Vasc. Endovasc. Surg.* **2004**, *38* (1), 11−23.

(2) Esteban, V.; Mendez-Barbero, N.; Jimenez-Borreguero, L. J.; Roque, M.; Novensa, L.; Garcia-Redondo, A. B.; Salaices, M.; Vila, L.; Arbones, M. L.; Campanero, M. R.; Redondo, J. M. Regulator of calcineurin 1 mediates pathological vascular wall remodeling. *J. Exp. Med.* **2011**, *208* (10), 2125−39.

(3) Autieri, M. V. Allograft-induced proliferation of vascular smooth muscle cells: potential targets for treating transplant vasculopathy. *Curr. Vasc. Pharmacol.* **2003**, *1* (1), 1−9.

(4) Hong, Y. J.; Jeong, M. H.; Song, S. J.; Sim, D. S.; Kim, J. H.; Lim, K. S.; Hachinohe, D.; Ahmed, K.; Hwang, S. H.; Lee, M. G.; Ko, J. S.; Park, K. H.; Yoon, H. J.; Yoon, N. S.; Kim, K. H.; Park, H. W.; Ahn, Y.; Cho, J. G.; Cho, D. L.; Park, J. C.; Kang, J. C. Effects of ramiprilat-coated stents on neointimal hyperplasia, inflammation, and arterial healing in a porcine coronary restenosis model. *Korean Circ. J.* **2011**, *41* (9), 535−41.

(5) Regan, C. P.; Adam, P. J.; Madsen, C. S.; Owens, G. K. Molecular mechanisms of decreased smooth muscle differentiation marker expression after vascular injury. *J. Clin. Invest.* **2000**, *106* (9), 1139−47.

(6) Pollman, M. J.; Hall, J. L.; Gibbons, G. H. Determinants of vascular smooth muscle cell apoptosis after balloon angioplasty injury. Influence of redox state and cell phenotype. *Circ. Res.* **1999**, *84* (1), 113−21.

(7) Szocs, K.; Lassegue, B.; Sorescu, D.; Hilenski, L. L.; Valppu, L.; Couse, T. L.; Wilcox, J. N.; Quinn, M. T.; Lambeth, J. D.; Griendling, K. K. Upregulation of Nox-based NAD(P)H oxidases in restenosis after carotid injury. *Arterioscler. Thromb. Vasc. Biol.* **2002**, *22* (1), 21−7.

(8) Lim, Y.; Tudev, M.; Park, E. S.; Kim, W. S.; Lim, I. H.; Lee, M. Y.; Lee, H.; Jung, J. K.; Hong, J. T.; Yoo, H. S.; Lee, M. K.; Pyo, M. Y.; Yun, Y. P. Inhibitory effects of OD 78 [3-(4-bromo-phenoxy)-4,5-dihydroxybenzoic acid-methyl ester] on the proliferation and migration of TNF-alpha-induced rat aortic smooth muscle cells. *Arch. Pharmacal Res.* **2011**, *34* (7), 1191−9.

(9) Lee, K. J.; Hinek, A.; Chaturvedi, R. R.; Almeida, C. L.; Honjo, O.; Koren, G.; Benson, L. N. Rapamycin-eluting stents in the arterial duct: experimental observations in the pig model. *Circulation* **2009**, *119* (15), 2078−85.

(10) Kim, H. J.; Cha, B. Y.; Choi, B.; Lim, J. S.; Woo, J. T.; Kim, J. S. Glyceollins inhibit platelet-derived growth factor-mediated human arterial smooth muscle cell proliferation and migration. *Br. J. Nutr.* **2011**, 1−12.

(11) Chen, H. W.; Huang, H. C. Effect of curcumin on cell cycle progression and apoptosis in vascular smooth muscle cells. *Br. J. Pharmacol.* **1998**, *124* (6), 1029−40.

(12) Jang, H. S.; Nam, H. Y.; Kim, J. M.; Hahm, D. H.; Nam, S. H.; Kim, K. L.; Joo, J. R.; Suh, W.; Park, J. S.; Kim, D. K.; Gwon, H. C. Effects of curcumin for preventing restenosis in a hypercholesterolemic rabbit iliac artery stent model. *Catheterization Cardiovasc. Interventions* **2009**, *74* (6), 881−8.

(13) Lopez-Lazaro, M. Anticancer and carcinogenic properties of curcumin: considerations for its clinical development as a cancer chemopreventive and chemotherapeutic agent. *Mol. Nutr. Food Res.* **2008**, *52* (Suppl. 1), S103−27.

(14) Jayaprakasha, G. K.; Jagan Mohan Rao, L.; Sakariah, K. K. Improved HPLC method for the determination of curcumin, demethoxycurcumin, and bisdemethoxycurcumin. *J. Agric. Food Chem.* **2002**, *50* (13), 3668−72.

(15) Kim, D. S.; Park, S. Y.; Kim, J. K. Curcuminoids from Curcuma longa L. (Zingiberaceae) that protect PC12 rat pheochromocytoma and normal human umbilical vein endothelial cells from betaA(1−42) insult. *Neurosci. Lett.* **2001**, *303* (1), 57−61.

(16) Betancor-Fernandez, A.; Perez-Galvez, A.; Sies, H.; Stahl, W. Screening pharmaceutical preparations containing extracts of turmeric rhizome, artichoke leaf, devil's claw root and garlic or salmon oil for antioxidant capacity. *J. Pharm. Pharmacol.* **2003**, *55* (7), 981−6.

(17) Yadav, V. R.; Suresh, S.; Devi, K.; Yadav, S. Effect of cyclodextrin complexation of curcumin on its solubility and antiangiogenic and anti-inflammatory activity in rat colitis model. *AAPS PharmSciTech* **2009**, *10* (3), 752−62.

(18) Quitschke, W. W. Differential solubility of curcuminoids in serum and albumin solutions: implications for analytical and therapeutic applications. *BMC Biotechnol.* **2008**, *8*, 84.

(19) Ruby, A. J.; Kuttan, G.; Babu, K. D.; Rajasekharan, K. N.; Kuttan, R. Anti-tumour and antioxidant activity of natural curcuminoids. *Cancer Lett.* **1995**, *94* (1), 79−83.

(20) Tiyaboonchai, W.; Tungpradit, W.; Plianbangchang, P. Formulation and characterization of curcuminoids loaded solid lipid nanoparticles. *Int. J. Pharm.* **2007**, *337* (1−2), 299−306.

(21) Anand, P.; Thomas, S. G.; Kunnumakkara, A. B.; Sundaram, C.; Harikumar, K. B.; Sung, B.; Tharakan, S. T.; Misra, K.; Priyadarsini, I. K.; Rajasekharan, K. N.; Aggarwal, B. B. Biological activities of curcumin and its analogues (Congeners) made by man and Mother Nature. *Biochem. Pharmacol.* **2008**, *76* (11), 1590−611.

(22) Vemula, P. K.; Li, J.; John, G. Enzyme catalysis: tool to make and break amygdalin hydrogelators from renewable resources: a delivery model for hydrophobic drugs. *J. Am. Chem. Soc.* **2006**, *128* (27), 8932−8.

(23) Ma, Z.; Shayeganpour, A.; Brocks, D. R.; Lavasanifar, A.; Samuel, J. High-performance liquid chromatography analysis of curcumin in rat plasma: application to pharmacokinetics of polymeric micellar formulation of curcumin. *Biomed. Chromatogr.* **2007**, *21* (5), 546−52.

(24) Liu, K.-H.; Chen, S.-Y.; Liu, D.-M.; Liu, T.-Y. Self-Assembled Hollow Nanocapsule from Amphiphatic Carboxymethyl-hexanoyl Chitosan as Drug Carrier. *Macromolecules* **2008**, *41* (17), 6511−6.

(25) Liu, T. Y.; Chen, S. Y.; Lin, Y. L.; Liu, D. M. Synthesis and characterization of amphiphatic carboxymethyl-hexanoyl chitosan hydrogel: water-retention ability and drug encapsulation. *Langmuir* **2006**, *22* (23), 9740−5.

(26) Braconi, C.; Meng, F.; Swenson, E.; Khrapenko, L.; Huang, N.; Patel, T. Candidate therapeutic agents for hepatocellular cancer can be identified from phenotype-associated gene expression signatures. *Cancer* **2009**, *115* (16), 3738−48.

(27) D'Souza, S. S.; DeLuca, P. P. Methods to assess in vitro drug release from injectable polymeric particulate systems. *Pharm. Res.* **2006**, *23* (3), 460−74.

(28) Watson, P.; Jones, A. T.; Stephens, D. J. Intracellular trafficking pathways and drug delivery: fluorescence imaging of living and fixed cells. *Adv. Drug Delivery Rev.* **2005**, *57* (1), 43−61.

(29) Nam, H. Y.; Kwon, S. M.; Chung, H.; Lee, S. Y.; Kwon, S. H.; Jeon, H.; Kim, Y.; Park, J. H.; Kim, J.; Her, S.; Oh, Y. K.; Kwon, I. C.; Kim, K.; Jeong, S. Y. Cellular uptake mechanism and intracellular fate

of hydrophobically modified glycol chitosan nanoparticles. *J. Controlled Release* **2009**, *135* (3), 259−67.
(30) Liu, Y.; Dolence, J.; Ren, J.; Rao, M.; Sreejayan, N. Inhibitory effect of dehydrozingerone on vascular smooth muscle cell function. *J. Cardiovasc. Pharmacol.* **2008**, *52* (5), 422−9.
(31) Liu, Y.; Ibricevic, A.; Cohen, J. A.; Cohen, J. L.; Gunsten, S. P.; Frechet, J. M.; Walter, M. J.; Welch, M. J.; Brody, S. L. Impact of hydrogel nanoparticle size and functionalization on in vivo behavior for lung imaging and therapeutics. *Mol. Pharmaceutics* **2009**, *6* (6), 1891−902.
(32) An, Z.; Shi, Q.; Tang, W.; Tsung, C.-K.; Hawker, C. J.; Stucky, G. D. Facile RAFT Precipitation Polymerization for the Microwave-Assisted Synthesis of Well-Defined, Double Hydrophilic Block Copolymers and Nanostructured Hydrogels. *J. Am. Chem. Soc.* **2007**, *129* (46), 14493−9.
(33) Lo, C. L.; Lin, K. M.; Hsiue, G. H. Preparation and characterization of intelligent core-shell nanoparticles based on poly(D,L-lactide)-g-poly(N-isopropyl acrylamide-co-methacrylic acid). *J. Controlled Release* **2005**, *104* (3), 477−88.
(34) Verheul, R. J.; van der Wal, S.; Hennink, W. E. Tailorable Thiolated Trimethyl Chitosans for Covalently Stabilized Nanoparticles. *Biomacromolecules* **2010**, *11* (8), 1965−71.
(35) Bachelder, E. M.; Beaudette, T. T.; Broaders, K. E.; Dashe, J.; Fréchet, J. M. J. Acetal-Derivatized Dextran: An Acid-Responsive Biodegradable Material for Therapeutic Applications. *J. Am. Chem. Soc.* **2008**, *130* (32), 10494−5.
(36) Bachelder, E. M.; Beaudette, T. T.; Broaders, K. E.; Fréchet, J. M. J.; Albrecht, M. T.; Mateczun, A. J.; Ainslie, K. M.; Pesce, J. T.; Keane-Myers, A. M. In Vitro Analysis of Acetalated Dextran Microparticles as a Potent Delivery Platform for Vaccine Adjuvants. *Mol. Pharmaceutics* **2010**, *7* (3), 826−35.
(37) Alexander, V, K. Polymer genomics: An insight into pharmacology and toxicology of nanomedicines. *Adv. Drug Delivery Rev.* **2006**, *58* (15), 1597−1621.
(38) Rothenfluh, D. A.; Hubbell, J. A. Integration column: Biofunctional polymeric nanoparticles for spatio-temporal control of drug delivery and biomedical applications. *Integr. Biol.* **2009**, *1* (7), 446−51.
(39) Hassani, L. N.; Hendra, F.; Bouchemal, K. Auto-associative amphiphilic polysaccharides as drug delivery systems. *Drug Discovery Today* **2012**, *17* (11−12), 608−14.
(40) Liu, T. Y.; Lin, Y. L. Novel pH-sensitive chitosan-based hydrogel for encapsulating poorly water-soluble drugs. *Acta Biomater.* **2010**, *6* (4), 1423−9.
(41) Wang, Y. J.; Chien, Y. C.; Wu, C. H.; Liu, D. M. Magnolol-loaded core-shell hydrogel nanoparticles: drug release, intracellular uptake, and controlled cytotoxicity for the inhibition of migration of vascular smooth muscle cells. *Mol. Pharmaceutics* **2011**, *8* (6), 2339−49.
(42) He, Y.; Huang, Y.; Cheng, Y. Structure Evolution of Curcumin Nanoprecipitation from a Micromixer. *Cryst. Growth Des.* **2010**, *10* (3), 1021−4.
(43) Prabaharan, M.; Reis, R. L.; Mano, J. F. Carboxymethyl chitosan-graft-phosphatidylethanolamine: Amphiphilic matrices for controlled drug delivery. *React. Funct. Polym.* **2007**, *67* (1), 43−52.
(44) Pae, H. O.; Jeong, G. S.; Jeong, S. O.; Kim, H. S.; Kim, S. A.; Kim, Y. C.; Yoo, S. J.; Kim, H. D.; Chung, H. T. Roles of heme oxygenase-1 in curcumin-induced growth inhibition in rat smooth muscle cells. *Exp. Mol. Med.* **2007**, *39* (3), 267−77.
(45) Kim, J. H.; Shim, J. S.; Lee, S. K.; Kim, K. W.; Rha, S. Y.; Chung, H. C.; Kwon, H. J. Microarray-based analysis of anti-angiogenic activity of demethoxycurcumin on human umbilical vein endothelial cells: crucial involvement of the down-regulation of matrix metalloproteinase. *Jpn. J. Cancer Res.* **2002**, *93* (12), 1378−85.
(46) Rutherford, C.; Martin, W.; Salame, M.; Carrier, M.; Anggard, E.; Ferns, G. Substantial inhibition of neo-intimal response to balloon injury in the rat carotid artery using a combination of antibodies to platelet-derived growth factor-BB and basic fibroblast growth factor. *Atherosclerosis* **1997**, *130* (1−2), 45−51.
(47) Slepian, M. J.; Massia, S. P.; Dehdashti, B.; Fritz, A.; Whitesell, L. Beta3-integrins rather than beta1-integrins dominate integrin-matrix interactions involved in postinjury smooth muscle cell migration. *Circulation* **1998**, *97* (18), 1818−27.
(48) Iversen, T.-G.; Skotland, T.; Sandvig, K. Endocytosis and intracellular transport of nanoparticles: Present knowledge and need for future studies. *Nano Today* **2011**, *6* (2), 176−85.
(49) Chithrani, B. D.; Chan, W. C. W. Elucidating the Mechanism of Cellular Uptake and Removal of Protein-Coated Gold Nanoparticles of Different Sizes and Shapes. *Nano Lett.* **2007**, *7* (6), 1542−50.
(50) Brodsky, F. M.; Chen, C. Y.; Knuehl, C.; Towler, M. C.; Wakeham, D. E. Biological basket weaving: formation and function of clathrin-coated vesicles. *Annu. Rev. Cell Dev. Biol.* **2001**, *17*, 517−68.
(51) Watson, P.; Jones, A. T.; Stephens, D. J. Intracellular trafficking pathways and drug delivery: fluorescence imaging of living and fixed cells. *Adv. Drug Delivery Rev.* **2005**, *57* (1), 43−61.
(52) Yu, Y. M.; Lin, H. C. Curcumin prevents human aortic smooth muscle cells migration by inhibiting of MMP-9 expression. *Nutr., Metab. Cardiovasc. Dis.* **2010**, *20* (2), 125−32.
(53) Parsons, J. T. Focal adhesion kinase: the first ten years. *J. Cell Sci.* **2003**, *116* (Part 8), 1409−16.
(54) Pan, C. H.; Chen, C. W.; Sheu, M. J.; Wu, C. H. Salvianolic acid B inhibits SDF-1alpha-stimulated cell proliferation and migration of vascular smooth muscle cells by suppressing CXCR4 receptor. *Vasc. Pharmacol.* **2012**, *56* (1−2), 98−105.